Aerogel-Coated Metal Nanoparticle Colloids as Novel Entities for the Synthesis of Defined Supported Metal Catalysts

Kai Man K. Yu,[†] Connie M. Y. Yeung,[†] David Thompsett,[‡] and Shik Chi Tsang*[,†]

Surface and Catalysis Research Centre, Department of Chemistry, University of Reading, Whiteknights, Reading RG6 6AD, U.K., and Johnson Matthey Technology Centre, Sonning Common, Reading RG4 9NH, U.K.

Received: November 21, 2002; In Final Form: February 3, 2003

Nanometer metal particles of tailored size (3−5 nm) and composition prepared via inverse microemulsion were encapsulated by ultrathin coatings (<2.5 nm) of inorganic porous aerogels covered with surface −OH groups. These composite materials formed metastable colloids in solvent(s), and the organic surfactant molecules were subsequently removed without leading to aggregation (the ethanolic colloid solution was shown to be stable against flocculation for at least weeks). We demonstrate that the totally inorganic-based composite colloids, after the removal of surfactant, can be anchored to conventional solid supports (γ-alumina, carbons) upon mixing. Application of a high temperature resulted in the formation of strong covalent linkages between the colloids and the support because of the condensation of surface groups at the interface. Detailed characterizations (X-ray diffraction (XRD), pore analysis, transmission electron microscopy (TEM), CO chemisorption) and catalytic testing (butane combustion) showed that there was no significant metal aggregation from the fine metal particles individually coated with porous aerogel oxide. Most of these metal sites on the coated nanoparticles with and without support are fully accessible by small molecules hence giving extremely active metal catalysts. Thus, the product and technology described may be suitable to synthesize these precursor entities of defined metal sizes (as inks) for wash coat/impregnation applications in catalysis. The advantages of developing inorganic nanocomposite chemical precursors are also discussed.

Introduction

Recent literature has shown the significance of using nanostructured materials in many areas. As a result, many governments/research councils have been advised to intensify their investment in "nanotechnology" for the coming years. The motivation has particularly stemmed from the recently observed unique electronic, optical, electrooptical, electrochemical, and catalytic properties associated with colloidal metal particles of controlled size and composition. There are a number of ways to synthesize metal particles with diameters between 1 and 20 nm. These include impregnation,[1,2] coprecipitation,[1] deposition−precipitation [1], sol−gel,[1,3,4] gas-phase organometallic deposition,[5] sonochemical,[6] microemulsion using organic stabilizing agents,[7] etc. Others specific methods such as laser ablation,[8] electrochemical,[9] and cross-linking[10] methods can also be found in the literature. For an excellent monodisperse size control, the use of organic stabilizing agents such as polymers, surfactants, and bulky ligand appendages as micelles or reversed micelles in liquid-phase creating "nanovessels" for tailoring metal size is regarded as one of the most promising routes.[11,12] The employments of water/oil microemulsion using organic stabilizers for the synthesis and direct use of ultrafine metal particles as colloid catalysts[13,14] and their dispersion in bulk sol−gel oxide matrixes[15,16] are documented.

In contrast, to our knowledge, few studies have been focused on the preparation of nanoparticles (metals and alloys of catalytic interests) for supported catalyst applications because the criteria for a practical supported nanosized catalyst are very different from those for other applications (specific catalyst−support interaction may be required, resistance to agglomerization, site isolation and good accessibility by substrate molecules, facilitated separation from products, mechanically robust, low synthetic cost, etc). In particular, the use of organic stabilizer in the microemulsion could interfere with the direct attachment of the particle to support (affecting the metal−support interactions) and increase the cost of synthesis, and their removal (highly exothermic upon firing in air) could cause agglomerization problems.

In this paper, nanosized metal cores (Pt, Pd, or Pt/Ag alloy), each coated with ultrathin aerogel porous overlayers (silica, ceria) of controlled size and composition, as novel chemical nanoprecursors are developed. These new but purely inorganic-based nanocomposite precursors, free from organic stabilizer, are shown to be colloidally metastable against agglomerization in ethanolic solution. They can be therefore supported on a wide variety of high surface area materials (alumina, silica, carbon) hence allowing separation of catalyst components from support with the major advantage of independent optimization of catalytic properties (protected nanoparticle with sol−gel coating of desired size, composition, porosity, metal−support interaction) from support properties (mechanical, thermal, flow, electrical, etc). Typically, Pt nanoparticles (average size of 5.1 nm), each encapsulated in porous silica aerogel coating (5 wt % metal, abbreviated as silogel@5%Pt), depositing on conventional γ-alumina as a composite catalyst for butane oxidation is demonstrated in Figure 1.

* To whom correspondence should be addressed. Dr. S. C. Edman Tsang. E-mail: scetsang@reading.ac.uk. Tel (fax): 00 44 118 9316346.
[†] University of Reading.
[‡] Johnson Matthey Technology Centre.

10.1021/jp0275239 CCC: $25.00
Published on Web 04/10/2003

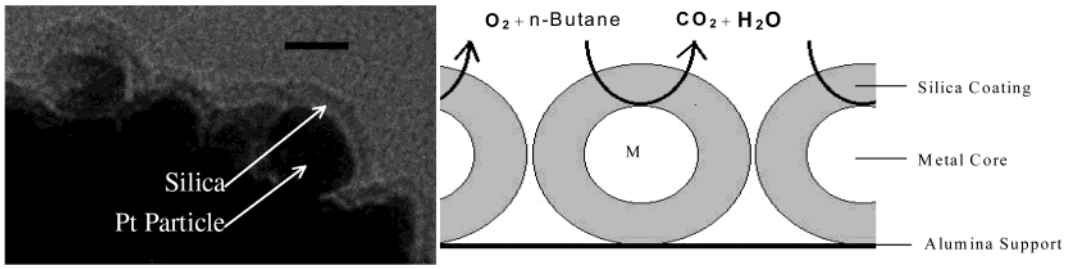

Figure 1. A TEM micrograph and a simplified model showing the alumina-supported silogel@5%Pt nanocomposites (scale bar = 5 nm).

Experimental Section

Materials. Pt, Pd, and Ag metal precursors were obtained as ammonium tetrachloroplatinate(II) (Pt assay 52.9%), sodium chloropalladite solution (Pd assay 13.2%), and silver nitrate (metal basis 99+%) from Johnson Matthey. Cetyltrimethylammonium bromide (CTAB), tetraethyl orthosilica (TEOS) 98%, hydrazine hydrate (99.9%), and cerium(III) nitrate hexahydrate (99%) from Aldrich were used as purchased. Toluene and ethanol from Fisher were AR grade. Ethanol was used without further purification; however, dried toluene was kept with molecular sieves before use.

Preparation and Characterizaion of the Catalysts. Formation of microemulsion was carried out using a small quantity of ionic surfactant, CTAB, and deionized water in excess dried toluene. Above critical micelle concentration (cmc), these three components form reversed micelles.[4,7] Because the size of such a micelle system is related to the ratio of water/surfactant (*W*) added, a minimum amount of water-to-surfactant ratio was used to reduce the size of the final nanocomposite synthesized therein.

Typically, the preparation of materials was done at room temperature, and silogel@Pt nanocomposite in microemulsion was prepared as follows (abbreviated as ME-method): 4.044 g of CTAB was added to dry toluene (150.0 cm^3) under vigorous stirring; a suspension of CTAB in toluene was formed immediately. Then an aqueous solution of Pt precursor salt, $(NH_4)_2PtCl_6$ (0.0958 g in 4.347 cm^3 DI water), was added dropwise to the suspension of CTAB in toluene, and the mixture was stirred to create aqueous micelles in the bulk toluene overnight. After that, 1.650 cm^3 of 1 M NaOH solution was added and the mixture was stirred for 2 h. Reduction of platinum ion was accomplished at ambient temperature by dropwise addition of excess hydrazine hydrate (0.50 cm^3). The solution turned black in color, but no precipitation was observed. This clearly implied that the reduction process does not significantly interfere with the stability of the microemulsion. TEOS (3.4637 g) was then added to the reaction mixture. Formation of the silica gel coating on the interface (the aqueous and toluene interface) of the micelle carrying the metal nanoparticle was expected to be achieved because the NaOH previously added is known to catalyze hydrolysis/condensation of the TEOS (nucleophilic substitution) to form a sol−gel coating. It was later found that the use of HCl instead (5 cm^3 in total mixed with ethanol) in the washing step produced almost no aggregation of colloid particles in solution (shown from the acoustic particle size analyzer). The composite colloids were allowed to age for 6 days at ambient conditions under a constant stirring of the solution. Using a similar technique, we prepared the silogel−ceria@Pt nanocomposite colloid in which an aqueous solution of Pt precursor salt (0.1944 g) and cerium(III) nitrate hexahydrate salt (0.6198 g) was used in the preparation of silo-10%ceriagel@5%Pt. The prepared silogel@Pt, silogel@Pd, and silo-ceriagel@Pt nanocomposites were then centrifuged and filtered using Celite glass. It was noted that the filtrate became colorless indicating that the composites were mostly retained in the residue after these treatments. The residue was then washed with excess toluene followed by hot ethanol. To extract all of the trapped surfactant molecules from the nanocomposites, the solid materials were then exhaustively washed in refluxing ethanol overnight twice. The final product material was filtered (centrifugally filtered) and dried in 333 K vacuum oven (or calcined for 3 h at 673 K).

Supporting silogel@Pt and silogel@Pd nanocomposites on conventional oxide and carbon materials was performed typically as follows: aluminum oxide (activated, acidic, standard grade, ca. 150 mesh) of stated quantity was added to the same silogel@Pt colloid solution described above and stirred overnight. The color of the resulting solution turned to light gray indicating that a substantial amount of silogel@Pt nanoparticles was immobilized onto the support. UV−vis spectroscopy was used to work out the nanocomposite loading on the support materials. The solid supported composites were then filtered, washed, surfactant extracted, and dried in the same manner as the unsupported composites.

Transmission electron microscopy (TEM) analysis was used to characterize particle size, structure, morphology, and composition through direct imaging, electron diffraction, and elemental analysis of selected areas. A Philips CM20 microscope operating at 200 kV equipped with an Oxford Instrument EDS6767 energy-dispersive X-ray analyzer (EDX) was used. High-resolution images were observed with a JEOL JEM-2010 transmission electron microscope operating at 200 kV. Sample was gently ground, suspended in 2-propanol, and placed on a carbon-coated copper grid after the evaporation of the solvent. Electron micrographs and EDX analyses of selected areas were taken.

X-ray powder diffraction (XRD) analysis of the samples was performed with a Simen Instrument X-ray diffractometer using Ni-filtered Cu $K\alpha_1$ of 1.540 56 Å radiation. Phase identifications of our samples were carried out by comparing the collected spectra with the published files from International Centre for Diffraction Data (JCPDS-1996). The average size of metal particle was calculated on the basis of peak broadening using the Scherrer equation. Instrumental peak broadening has also been taken into account.

Fourier-transform infrared spectra (FTIR) of samples were collected using KBr compressed pellets. This technique was mainly employed to identify the Al−O−Si linkage from the shifts of the wavenumber recorded as compared to the literature.[17]

Physical characterizations (porosity, surface area, pore distribution) of dried samples were carried out using standard N_2 Brunauer−Emmett−Teller (BET) method at a range of partial pressure at 77 K (Sorptometic 1990 from CE Instrument), and Barrett−Joyner−Halenda (BJH) method was used to elucidate the average pore size and distribution.

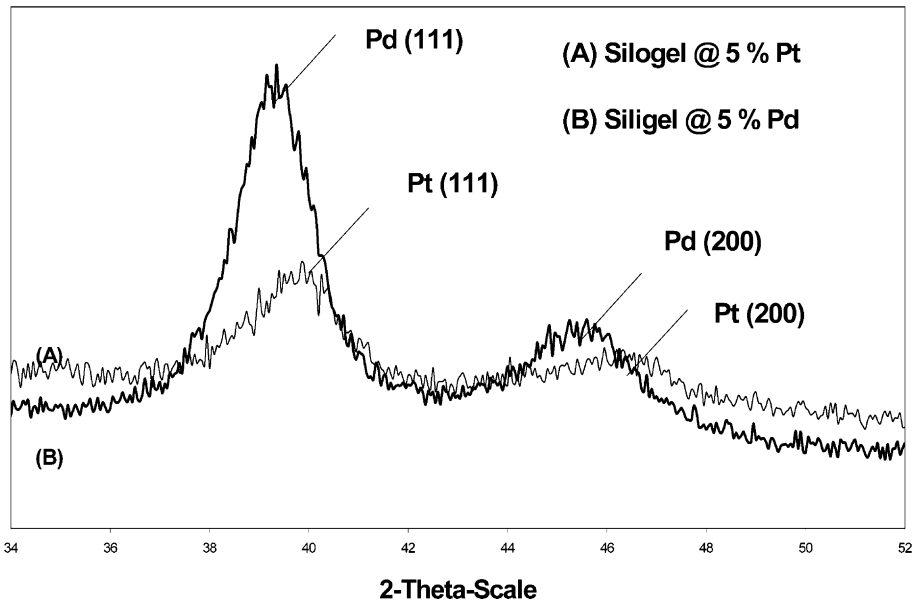

Figure 2. XRD spectra showing the nanosized Pt and Pd particles prepared by the ME method. The Pt {111} spacing and the Pd {111} spacing from XRD measurement were determined to be 2.26 ± 0.01 Å (2θ of 39.85°) and 2.29 ± 0.01 Å (2θ of 39.30°), respectively.

TABLE 1: A List of the Samples Prepared Using Water/Surfactant Ratio, $W = 30$, unless Otherwise Stated

sample	description	R^c	SA ($m^2\ g^{-1}$), (from N_2 BET)	average pore size (from BJH), nm	average inner metal particle size (from XRD), nm
1[a]	silogel@5%Pd		390.5	11.4	3.9
2[d]	silogel@16%Pd				9.8
3	silogel@5%Pt		193.9	3.8	4.8
4	silogel@5%Pt−Ag (Pt/Ag 1:1 w/w)				5.3
5	silo-10%ceria gel@5%Pt				(Pt) 5.5; (CeOx) wk
6	silo-5%ceria gel@5%Pt				
7	silogel@5%Pt−0.5[b]-alumina	0.5			4.8
8	silogel@5%Pt−1.0[b]-alumina	1	124.6	3.7	4.7
9	silogel@5%Pt−2.0[b]-alumina	2	123.4	3.7	5.1
10	silogel@10%Pt−1.0[b]-alumina	1	122.6	3.7	6.7
11	acid−silogel@5%Pt−0.2[b]-alumina	18	109.4	3.6	4.8
12	silica gel (grade 643, 200−425 mesh)		267.7		
13	activated acidic alumina (150 mesh)		133.6		

[a] Detailed comparison of particle size evaluated from TEM and CO chemisorption techniques. [b] Amount of alumina added (g) as support. [c] R = Al/Si weight ratio. [d] A water to surfactant molar ratio of $W = 70$ was used.

Apparatus and Procedure for the Catalytic Experiments. *n*-Butane catalytic oxidation (combustion) was conducted using our home-built microreactor where catalyst in powder form was placed. The microreactor was in the form of a quartz tube with an internal diameter of 5 mm where 0.01 g of catalyst was packed and sandwiched between two silica wool plugs. The packing height was about 2−3 mm. All samples were used as stated without any preactivation. The total gas flow rate used in a typical reaction was 60 cm^3/min. The feed gas was composed of a 1:1 mixture from two BOC special gas cylinders (one is calibrated as 7000 ppm of *n*-butane in air and the other is the pure air cylinder), each delivered at 30 cm^3/min by two individual mass flow controllers. The catalytic test at a particular temperature was complete in an isothermal environment before bringing up to the next set of higher temperatures. After the catalyst was stabilized with the feed gas at the desired temperature for about 30 min, the product gases were analyzed by a Perkin-Elmer AutoSystem XL gas chromatograph equipped with a methanator and a flame ionization detector (FID). A Carbosphere (Alltech) packed column (6 ft × $^1/_8$ in.) was used to separate CO, CO_2, and *n*-butane with nitrogen as the carrier gas. Under typical conditions, CO_2 was also exclusively produced from the total oxidation of *n*-butane with traces of CO and other hydrocarbons. The use of such a small amount of the composite catalysts in a fast reactant flow for butane combustion (the Gas hour space velocity, GHSV, is estimated to be 73 000 h^{-1}) is to ensure a good heat management of the catalyst bed without engaging in any possible run-away reactions (highly exothermic).

Results

Preparation of Unsupported Silogel@Monometallic Nanocomposites by the ME Method. Figure 2 shows typical XRD patterns of unsupported silogel@Pd and silogel@Pt samples prepared by our ME method using the same water/surfactant ratio, $W = 30$. As reference to the published XRD data of Pd (JCPDS-05-0681) and Pt (JCPDS-04-0802), respectively, the two most intense peaks in each XRD pattern corresponding to (111) and (200) interplanar separations of the noble metals were clearly visible from our samples though the peaks were very broad indicative of small particle size. There were no distinctive peaks detected due to the silica sol−gel coating. Using the water/surfactant ratio of W, we determined that the average diameter of Pd in the silogel@5%Pd sample was 3.9 nm (Table 1). This was calculated on the basis of the (111) peak broadening of Pd according to Scherrer's equation (taking account of instrumental broadening). The Pt particle size recorded using the same W

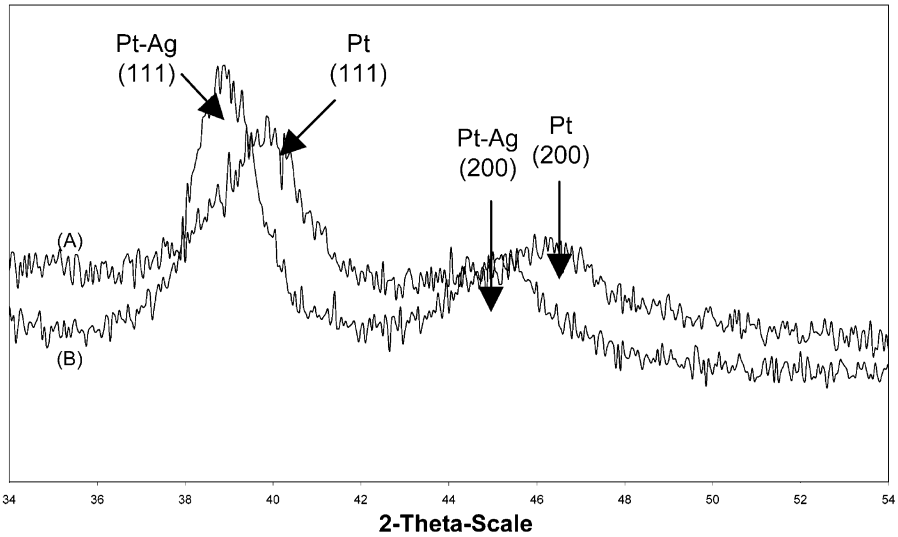

Figure 3. XRD spectra obtained from (A) silogel@5%Pt and (B) silogel@5%($Pt_{0.33}Ag_{0.67}$). The Ag−Pt {111} spacing and the Pt {111} spacing from the XRD measurements were determined to be 2.32 ± 0.01 and 2.26 ± 0.01 Å, respectively.

was 4.8 nm (Table 1), which was based on (111) of Pt broadening. With the exception of the experiments 2 and 10 in Table 1 in which higher metal loadings were used, the general particle size of 4.5 ± 0.8 nm was obtained using $W = 30$ for 5% metal content within the experimental errors. It is noted that using nonionic surfactant/water reversed micelle system ($w = 6$) Hanaoka et al.[16] were able to control the Rh particle to a similar size of 4−4.2 nm. In our case, by increasing our water/surfactant ratio to 70, we obtained an average size of 9.75 nm Pd particle with 16% metal loading (Table 1). Thus, our results agree with the observations that diameter of metal nanoparticles synthesized inside the micelle system depends on micelle diameter (size of the included material ≤ size of the aqueous core), which critically depends on the water/surfactant ratio used.[18,19] The subsequent application of the silica gel coating onto these micelle-stabilized metal nanoparticles does not seem to seriously alter the metal particle size. It is, however, noted that this technique could only indicate the average size of our metal cores (not the size distribution) and gives no information on the silica sol−gel coating because no distinctive peaks due to the silica were detected (indicative of its amorphous nature).

Unsupported Silogel@5%($Pt_{0.33}Ag_{0.67}$) Nanoparticles. We attempted to synthesize aerogel-coated alloy nanoparticles of controlled dimensions using our method. The synthesis of a truly alloy colloid (stabilized by surfactants) in which two metal atoms are homogeneously mixed within a nanoparticle is challenging, particularly with regard to their probable phase segregation under some preparation conditions; however, these nanoalloy particles show excellent hydrogenation activities.[20] Aqueous solutions of two metal precursors, ammonium tetrachloroplatinate and silver nitrate (with Pt/Ag = 1:0.92 w/w with Ag/Pt atomic ratio set at 2), were added into the reversed micelles instead of using one metal precursor as previously described. It is noted that Figure 3 shows a high but broad peak at 38.80° (2θ) with the d spacing determined to be 2.32 ± 0.01 Å. This does not resemble the Pt(111) of 39.85° obtained over the silogel@5%Pt (refer to Figures 2 and 3) or the Ag(111) of 38.10° over the Ag nanocolloid particles but with a clearly good agreement with the reported Pt−Ag alloy colloid.[18,21] Lattice constants of our new silica gel encapsulated Pt and Pt−Ag alloy particles calculated from the {111} lattice spacings (all with F. C. C. structure) are depicted in Table 2, along with the reported values for bulk metals and for uncoated colloids.[22] It is noted that the lattice constants of our silogel-coated Pt and the silogel-coated bimetallic Pt−Ag agreed within the error with the reported values of the corresponding Pt and $Pt_{0.33}Ag_{0.67}$ in colloid and in bulk forms. The lattice constant of our coated bimetallic nanoparticles also agreed with the value calculated on the basis of the assumption of Vegard's law, that is, the additivity of lattice constants for bimetallic alloy. It should be noted that the lattice spacings of our silogel-coated monometallic and bimetallic nanoparticles (and also the uncoated colloids) are somewhat (ca. 1%) smaller than those of bulk metals. This is presumably due to lattice contractions with decreasing particle size as reported for Cu and Ni clusters by extended X-ray absorption fine structure (EXAFS) measurements.[18]

TABLE 2: Lattice Constants of Silogel@5%Pt and Silogel@5%($Pt_{0.33}Ag_{0.67}$) Derived from the XRD Data Compared with the Literature Values of the Corresponding Pt, Ag, and $Pt_{0.33}Ag_{0.67}$ in Colloid and in Bulk Forms

nanocomposite	a, Å	metal/alloy	a, Å
silogel@5%Pt	3.91 ± 0.01	bulk Pt[22]	3.92
		colloid Pt[18]	3.91
		bulk Ag[22]	4.09
		colloid Ag[18]	4.04
silogel@5%($Pt_{0.33}Ag_{0.65}$)	4.02 ± 0.01	bulk $Pt_{0.33}Ag_{0.67}$[22]	4.03
		colloid $Pt_{0.33}Ag_{0.67}$[18]	4.00

On the basis of the XRD peak broadening, the average of the coated 5% $Pt_{0.33}Ag_{0.67}$ particle size was determined to be 5.3 nm, matching with the general particle size of 4.5 ± 0.8 nm that we obtained using $W = 30$ within the experimental error. To confirm the true alloy formation a direct HR-TEM imaging (Figure 4) of the $Pt_{0.33}Ag_{0.67}$ core was taken. Ag−Pt {111} spacing of 2.30 ± 0.02 Å is clearly visible, which is in excellent agreement with the XRD result. As a consequence, from evidences obtained by HR-TEM imaging and XRD measurement, the results strongly suggest that bimetallic alloy nanoparticles as $Pt_{0.33}Ag_{0.67}$ of the average size similar to monometallic nanoparticles using the same metal loading with no observed phase segregation can be synthesized from our technique.

One key point of this research is to demonstrate the existence of silogel coating embracing these particles despite the fact that the TEOS added onto the aqueous microemulsion in toluene should be hydrolyzed/condensed to form the nanocoating during their syntheses. As a result, detailed EDX analysis of the silogel@5%($Pt_{0.33}Ag_{0.67}$) sample has been performed using a nanoprobe to map five different areas randomly selected under the microscope (with a small spot size of ca. 27.5 nm in diameter

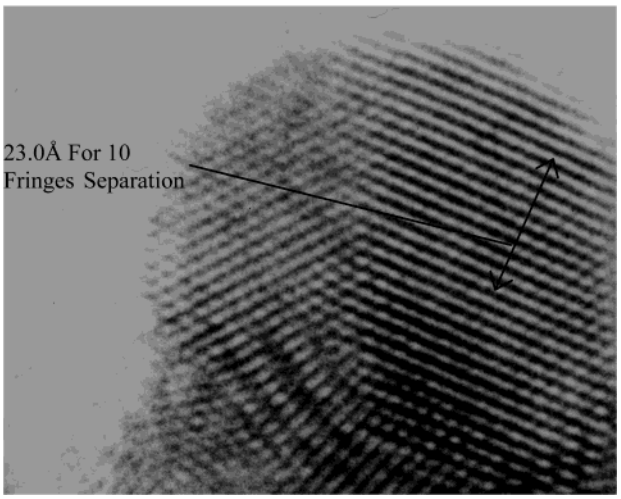

Figure 4. A direct HRTEM imaging of the Pt−Ag core showing the Pt−Ag {111} spacing of 2.30 ± 0.02 Å (scale bar of 23.0 Å where 10 lattice fringes are clearly visible).

for examining not more than five nanocomposite aggregates therein). It is noted that introduction of this sample onto a copper grid prior to placing them into the microscope was conducted using its ethanolic colloid solution (see Figure 7) after the surfactant removal. The typical spectrum and compiled results are shown in Figure 5 and Table 3, respectively. The multi-

TABLE 3: The Average Compositions of the Silogel@5%($Pt_{0.33}Ag_{0.67}$) of the Five Selected Areas Taking the ZAF Correction

	element wt % with respect to silica		
site of interest	Ag	Pt	Ag−Pt
1	2.28	2.54	4.82
2	2.70	2.73	5.43
3	2.02	2.14	4.16
4	2.92	2.91	5.83
5	2.32	2.52	4.84
avg wt % metal loading	2.45	2.57	5.02
SD	0.36	0.29	0.64

channel elemental analysis (Figure 5) clearly indicated that the sample gives the constant atomic ratios Si/O/Ag/Pt over the five selected areas. By taking the atomic number effect (Z), absorption (A), and fluorescence (F) corrections into account, we find that the calculated composition of each component in such small areas of examination (Table 3) agrees well with the total added ingredients within experimental errors (∼5 wt % alloy content, the rest being the SiO_2). It is accepted that the bare metal nanoparticles (hydrophobic) could not be stabilized in ethanol without a hydrophilic coating. Hence, these results clearly indicate homogeneously dispersed alloy particles coated with silica material.

Removal of Organic Surfactant Moieties. Because the key research was to investigate whether the monometallic or bimetallic nanoparticles can be stabilized in solution by the silica sol−gel coating without any involvement of the organic surfactant molecules, extraction of surfactant molecules was achieved as described in the Experimental Section. Thermogravimetric analysis (TGA) was used to investigate the levels of organic moieties present in the samples by recording their weight changes (and heat changes in the differential thermal analysis curves) upon their temperature ramping in air. Dried silogel@5%Pt samples before and after the surfactant extraction (reflux in ethanol) were studied. It is noted from Figure 6A that the silogel@5%Pt before the surfactant extraction shows a significant loss in weight (∼22%) associated with an exothermic peak at around 220−280 °C (started at 200 °C and finished at 300 °C). There were further minor weight losses at 385 °C (∼1%, endothermic) and 530 °C (∼0.5%). To identify these weight changes, a sample based on a physical mixture of surfactant (CTAB) and silogel was used for a comparative purpose (Figure 6B). It was found that the physical mixture also produced a sharp loss in weight at the same temperature regime (250−280 °C), clearly indicative of this exotherm associated with the combustion of surfactant molecules. The minor weight changes at the higher temperatures were also visible (at 395 and 520 °C), which are attributed to the dehydroxylation of silanol groups as observed in the literature.[23] It is important to note that the silogel@5%Pt composites, after the ethanol reflux (Figure 6C), showed less than 1% drop in weight at 220 °C; hence, a majority of surfactant molecules can be readily extracted despite the presence of the porous sol−gel coatings (akin to extraction of surfactant from MCM-41 silicate samples).

Transfer of Acid−Silogel@5%Pt onto Alumina. It is very interesting to note that colloidal silogel@5%Pt after the surfactant extraction could remain metastable in ethanol against flocculation (no deposition observed) indicative that the surface −OH on the silica sol−gel coating may stabilize the small particles in ethanol solution. The colloid solution appeared to be completely dark in color, and no residue was obtained as it passed through a filter paper (see Figure 7). The initial experiments showed that the colloidal organic-free silogel@5%Pt can be adsorbed onto high surface area carbon black, silica, and activated acidic alumina. A more detailed study was performed using activated acidic alumina as the support. It was

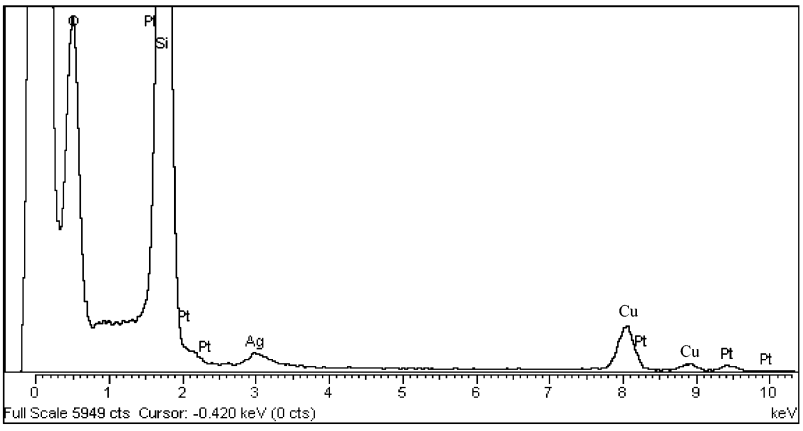

Figure 5. EDX analysis for silogel@5%($Pt_{0.33}Ag_{0.67}$) showing the homogeneous composition of Pt and Ag (5 wt %, Ag/Pt atomic ratio ≈ 2).

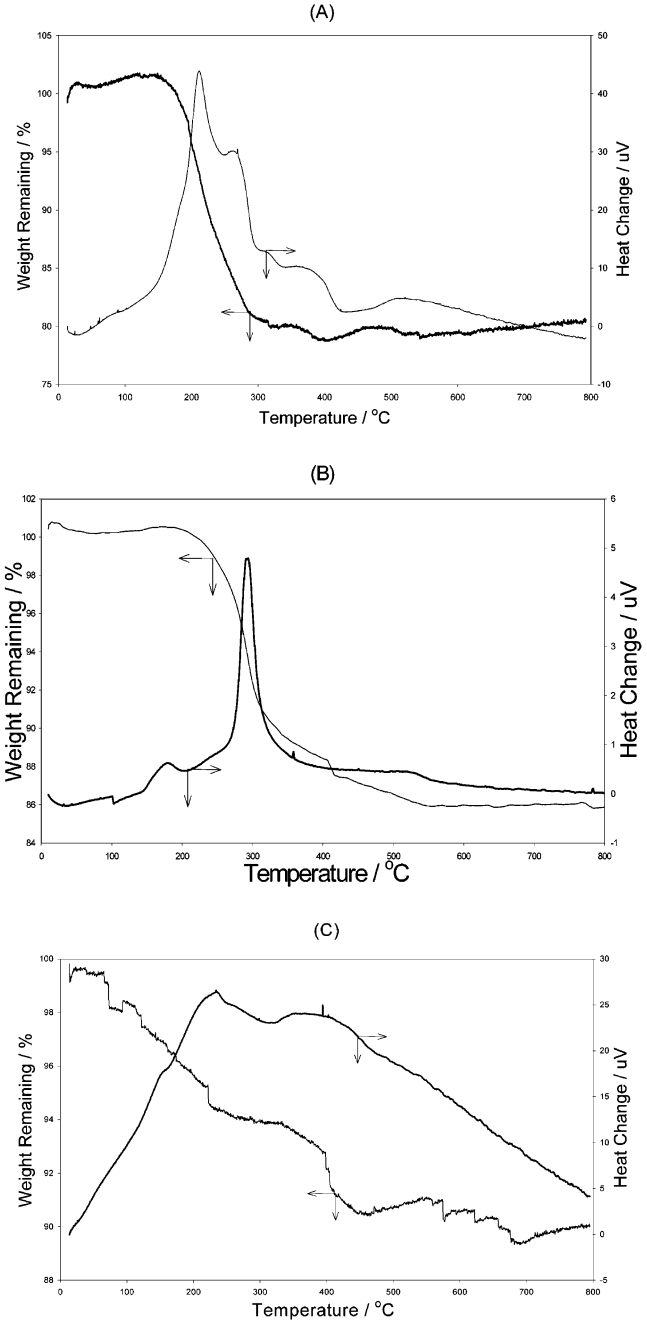

Figure 6. TGA showing the organic-contained (A) silogel@5%Pt prior to ethanol treatment, (B) a physical mixture of surfactant and silica gel, and (C) silogel@5%Pt extensively washed by ethanol.

found that a maximum of 186 mg of Pt/silica composites can be adsorbed per gram of activated γ alumina (BET N_2 surface area of 133.63 m^2 g^{-1}) used, which was extracted from the excess acid−silogel@5%Pt colloidal solution (0.0013 g/cm^3). This uptake value is high (~20 wt % worked out from the UV−vis spectra) though it is still below the theoretical monolayer coverage (assuming the close packing of composites on surface and that all of the surfaces are available). Thus the composites appear to distribute well on the alumina surface without their surface aggregation. Figure 7 shows clearly the changes of black colloidal silogel@5%Pt to a colorless solution (total adsorption) and the white alumina powder to gray in color. The result shown in Figure 7 was obtained after 4 h of stirring to ensure that the partitioning between the liquid phase and the solid support phase is readily established. For a shorter time (<30 min), there are clear indications that the solid adsorbed composites can be

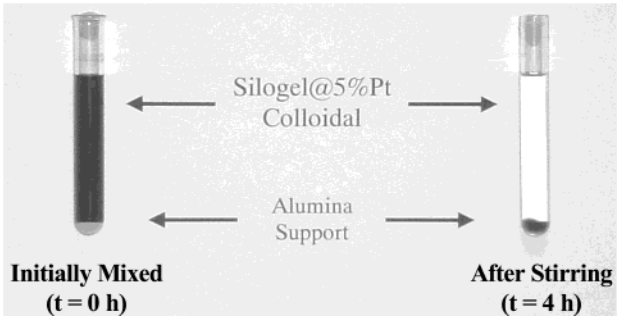

Figure 7. A photograph showing the impregnation of nanocomposites onto alumina.

reversibly released upon the use of acidified water/ethanol solution. This weak initial interaction could be due to the electrostatic effect, which was attributed to the difference in isoelectric points of the silica coat (negative at pH 7) and the alumina support (slightly positive at pH 7) possibly in the presence of a small amount of adsorbed water. However, it was observed that most of the nanocomposites could not be rinsed off from the alumina support with a pure ethanol solution (>80% from the UV−vis. analysis) after the nanocomposites were in contact with the alumina for a prolonged period of time (>1 h).

TEM Characterization. Figure 8A−C presents the TEM micrographs of the unsupported aerogel@metal nanocomposites. It is noted that the average particle sizes as estimated by the TEM micrographs were generally consistent with those calculated from the XRD peak broadening. It is interesting to point out that the shape of most of the particles was nearly spherical. Figure 8E presents a particle size histogram for the typical silogel@5%Pt. The result shows that the size distribution of the inner core metal is unimodal giving an average particle size of 3.4 nm with a deviation of 0.4 nm, which agrees reasonably closely with the metal nanoparticles of 3.5 ± 0.8 nm evaluated from the XRD data using the typical water/surfactant ratio. Closer examination of the micrographs reveals that the diameter distribution was extremely sharp, suggesting that the ME technique is able to tailor metal size approaching monodispersity. The spherical particle shape and the sharp unimodal size distribution are consistent with the previous observations that these nanoparticles are synthesized inside the micelles. From the contrast of the images in the micrographs (Figures 1 and 8A−D)), the dense (dark) metallic clusters are clearly found all enclosed individually by a (light) sol−gel porous coating of ca. 2.50 ± 0.02 nm (Figure 1) thickness depending on the water/surfactant content.

CO Chemisorption. CO chemisorption was conducted to determine the inner metal surface of the typical unsupported silogel@5%Pd having a metal inner core size of 3.9 nm (XRD). It was also attempted to determine the average Pd particle size from the corresponding metal surface area to confirm the XRD and TEM results with another independent technique. The measurements were conducted at room temperature by using a pulse flow technique with a CO loop volume of ca. 0.25 cm^3. Prior to the measurement, each sample (about 0.15 g) was prereduced by 33% hydrogen in helium at 573 K for 30 min. With a thermal conductivity detector (TCD) as the detector, the measurements were performed with an injection of 0.25 cm^3 of CO after the samples were cooled to room temperature under the flow of hydrogen/helium. The metal dispersion was calculated by assuming a stoichiometry CO/Pd = 1, which also assumes a linear mode of adsorbed CO is formed on Pd. It is known that some degree of error in the size estimation will be

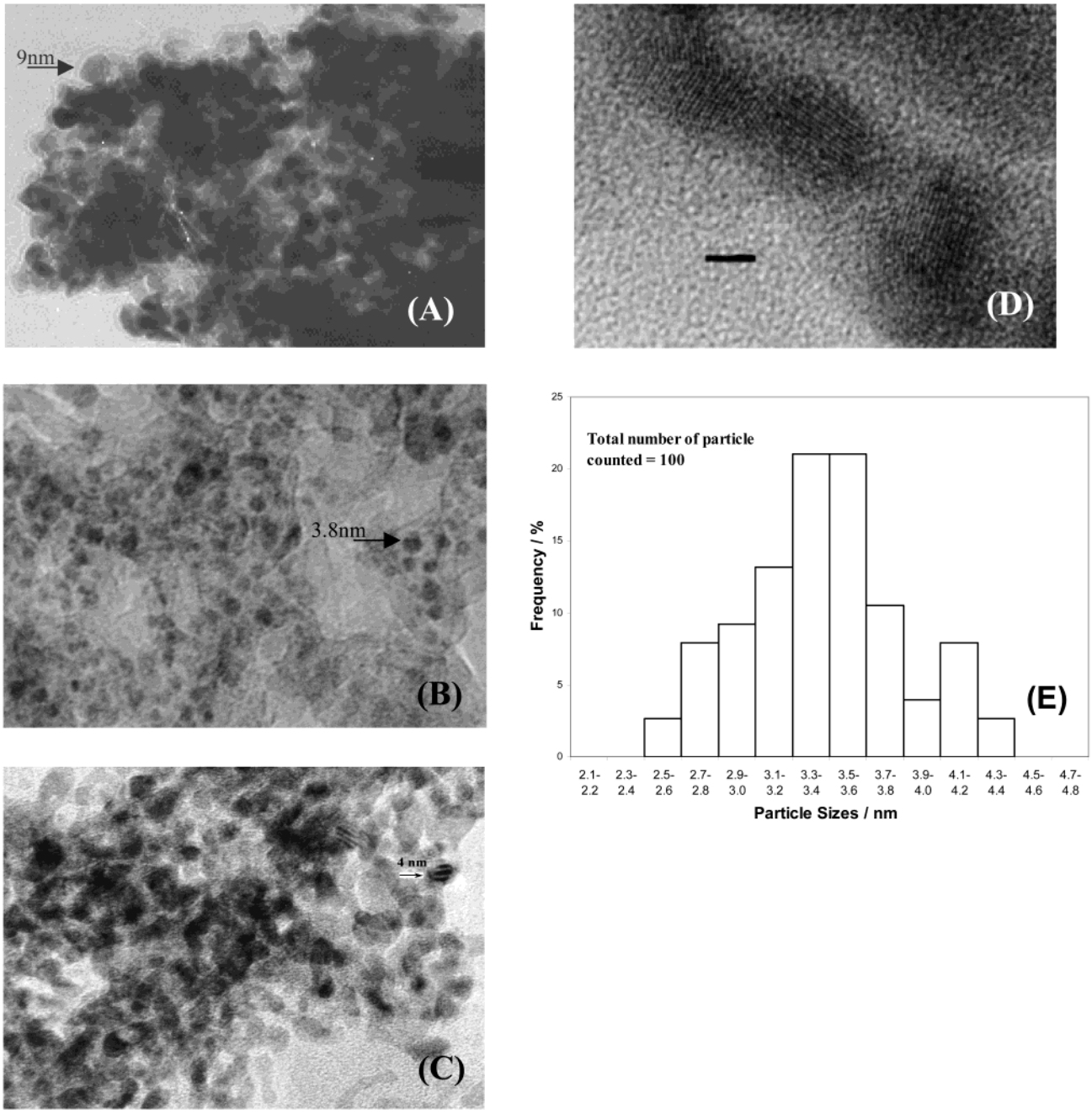

Figure 8. TEM images for samples (A) silogel@16%Pd, (B) silogel@5%Pt, (C) acid−silogel@5%Pt, and (D) silogel@5%Pt−1-g-alumina (scale Bar = 2 nm) and (E) a size histogram of the silogel@5%Pt sample showing the core Pt with an average size of 3.4 ± 0.4 nm (standard deviation).

introduced when this assumption cannot apply (especially when dealing with a large particle). Nevertheless, this assumption was generally accepted to be valid on SiO_2-supported Pd nanoparticles with a similar metal size as ours.[24] Thus, the metal surface area was found to be 69.6 $m^2\ g^{-1}$. On the basis of the fact that most particles are spherical in shape (as seen from TEM micrographs), the average crystallite size was then calculated to be 3.59 nm. This result is in an excellent agreement with the result obtained from XRD and TEM imaging within experimental errors. The other important fact worth mentioning is that such a good agreement of the dimension of the unsupported sol−gel encapsulated monodispersed metal particles clearly suggests that the aerogel-coated composites are fully accessible by small molecules such as H_2 and CO. Other CO chemisorption experiments, on the other hand, revealed that the average Pt crystallite size was 6.9 nm (XRD = 4.8 nm, TEM = ∼5 nm) in the acid−silogel@5%Pt supported on the 0.2-g alumina sample (refer to Table 1). The precise reason for the significant discrepancy between the considerably larger average particle size determined by CO chemisorption and the smaller size determined by the XRD and the TEM is not yet known. It is thought that this may be due to inaccessibility of some metal surface by CO when these nanocomposites were deposited onto the alumina. It is possible that such small supported nanoparticles may sustain few layers of external oxide shells somehow assisted by the support(s), although great care in preventing reoxidization of these H_2 prereduced particles prior CO chemisorption was taken. These oxide coats will certainly reduce the CO chemisorption value hence over-estimating the size of these particles. The other possibility is that some of the porous silica sol−gel coating forms an impermeable interface with the alumina when exposed to a high temperature during the prereduction period (sintering) hence reducing the accessibility of these nanocomposites by the CO molecules.

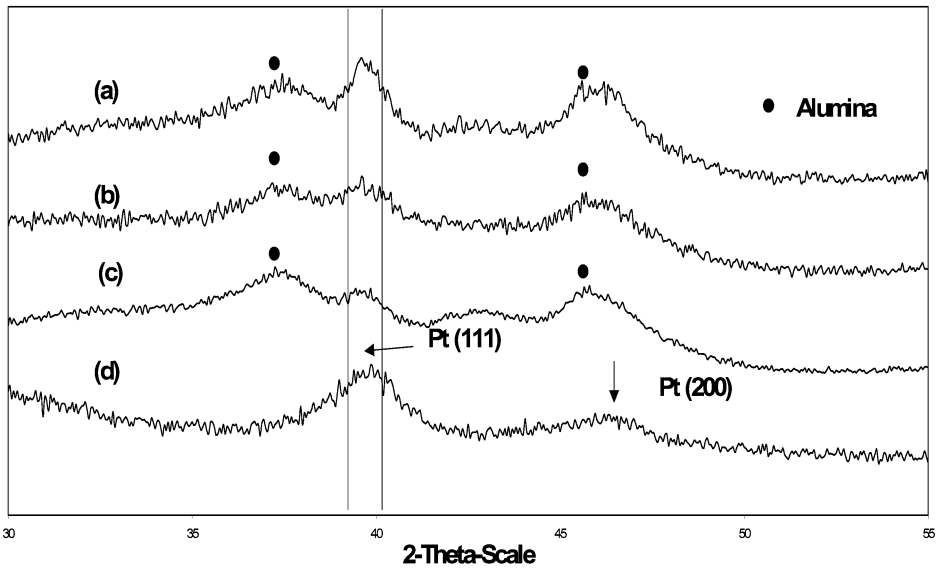

Figure 9. XRD spectra showing different loading of catalytic precursor: (a) silogel@5%Pt supported onto 1.0 g of alumina, $R = 1$; (b) silogel@5%Pt supported onto 2.0 g of alumina, $R = 2$; (c) acid−silogel@5%Pt−alumina $R = 18$; (d) silogel@5%Pt, $R = 0$.

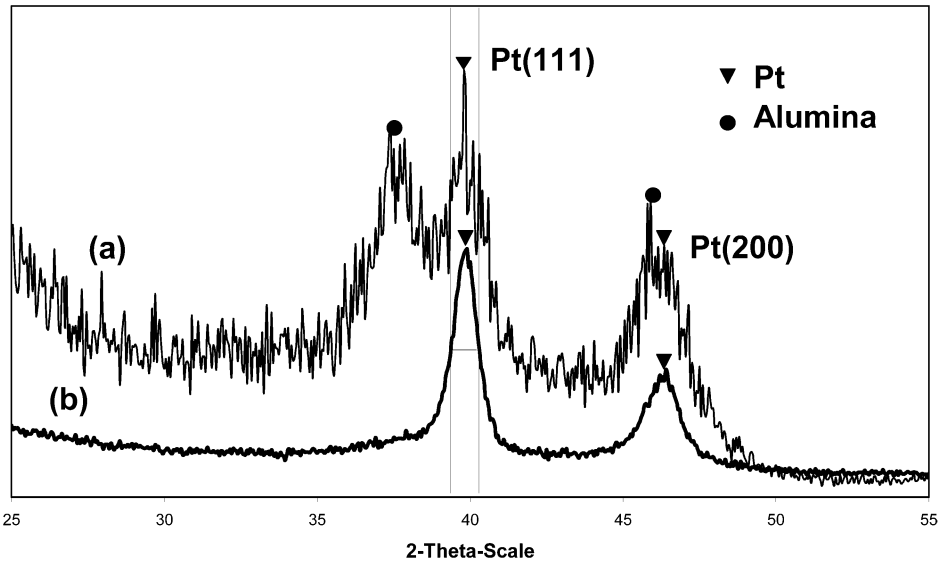

Figure 10. Effect on particle size after doubling the Pt salt concentration in microemulsion. (A) silogel@5%Pt supported onto 1.0^b − alumina, (B) silogel@10%Pt supported onto 1.0^b − alumina.

Solid-Supported Aerogel@Metal Nanocomposites. Figure 9a−d shows the XRD patterns of the silogel@5%Pt nanocomposites before and after their attachment to the conventional high surface area alumina support. Figure 9d shows clearly the two broad peaks due to the (111) and (200) of Pt of the unsupported composites with inner metal core of 4.8 nm. High surface area alumina does not produce any XRD feature at around 40° (2θ) such that (111) Pt is chosen to study the loading effect of the particle size (HR-TEM in Figure 8D shows that the Pt particle size is about 4.2 nm in the silogel@5%Pt−1-g alumina sample.) It was found that despite a wide range of composite loading to the alumina (R = Al/Si ratios from 0.5 to 18) the inner Pt nanoparticle size retained more or less the same size (refer to Table 1) showing no metal aggregation due to a possible rupture of the coating upon attachment to the support. In addition, from Figure 10, it can be seen that the half peak width of the Pt particle from the silogel@5%Pt/alumina spectrum (intensity enlarged) is larger than that of the silogel@10%Pt/alumina in which twice the Pt precursor concentration in the same micelles was used. The calculated Pt metal sizes from the peak broadening in these two cases were 4.8 and 6.7 nm, respectively (Table 1). Thus, it is apparent that the metal size can be controlled by either the concentration of Pt precursor (Figure 10) or the water/surfactant ratios used (Table 1).

FTIR. FTIR was used to characterize the linkages between the alumina support and aerogel@metal nanocomposites before and after calcination. Figure 11D,E shows the IR absorption spectra of pure silica gel and alumina support, respectively. Particularly, the region from 1400 to 800 cm^{-1} where the dominant features of asymmetric vibration modes of Si−O(A) are found is closely examined. When A = Si (in pure silica), the corresponding asymmetric vibration is at about 1085 cm^{-1} and when A = H (a large quantity of surface hydroxyl), the asymmetric vibration of Si−O(H) is at nearly 975 cm^{-1}.[17] Thus, the position of this asymmetric vibration Si−O mode depends on the second neighbor atoms, which is generally accepted in sol−gel synthesis[25] as the way to determine whether atomic mixing of Al into SiO_2 matrix can be achieved as [Si−O−(Al)] during aging of the Al and Si precursors together at room temperature via examination of the shift in the wavelength. Substitution of Al among the Si−O network will attenuate the

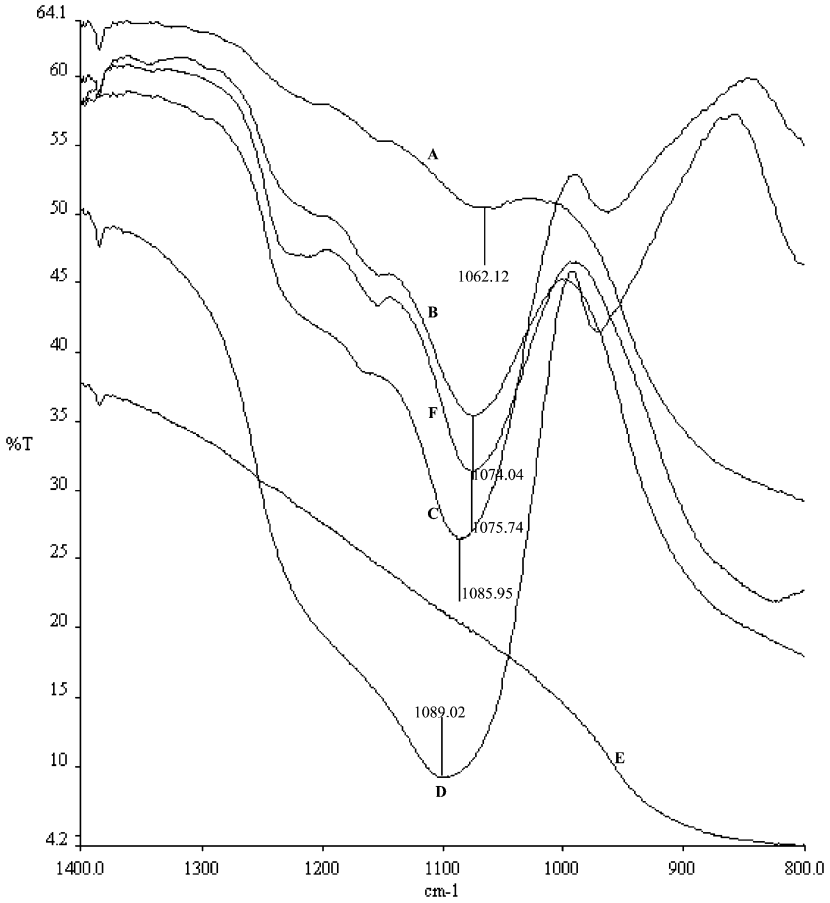

Figure 11. The Si−O band shift due to the presence of Al−O−Si bonding: (A) acid−silogel@5%Pt−alumina $R = 18$; (B) silogel@5%Pt−2-alumina $R = 2$; (C) silogel@5%Pt $R = 0$; (D) silica gel; (E) alumina support; (F) calcined silogel@5%Pt−2-alumina $R = 2$.

stretching wavenumber (due to Si−O(Al)).[25] It is believed that when Al^{3+} (a Lewis acid site of the size considerably smaller than Si) is the second neighbor of the Si−O, the Al^{3+} will attract the oxygen more strongly than Si. Hence, the Si−O(Al) asymmetric stretching would be located at a lower k value than that of Si−O(Si). Figure 11C,D represents those samples without the addition of alumina support. The Si−O(Si) asymmetric stretching bands located at ∼1085 cm^{-1} and Si−O(H) hydroxyl group stretching bands located at ∼980 cm^{-1} (a large quantity of terminal hydroxyl groups for these small sol−gel silica samples) are clearly visible. On the other hand, Figure 11A,B,F shows clearly the disappearance of Si−O(H) hydroxyl group stretching bands at ∼980 cm^{-1} associated with a progressive shift of the Si−O asymmetric stretching band to a lower wavenumbers on increasing the alumina support content. Thus, the presence and increasing degree of covalent linkages of the Si−O(Al) due to the condensation of the surface −OH group of the nanocomposites and the support (Al−OH) is therefore evident. It is noted that the well-dispersed alumina-supported silogel-coated nanocomposites with a high aluminum content ($R = 18$) account for more Si−O(Al) linkages and consequently a larger degree of shift. These are taken as evidence for the formation of chemical linkage between the sol−gel silica coating with the alumina support when the two materials were allowed to mix for a prolonged period of time. It is also noted that Figure 11F represents the silogel@5%Pt−2-g alumina sample calcined at 623 K, which shows no apparent change when compared with the spectrum of the Figure 11B. This fact clearly suggests that the formation of Si−O−Al linkage from the dehydroxylation (gelation) reaction of the Si−OH and Al−OH can readily occur at ambient conditions.

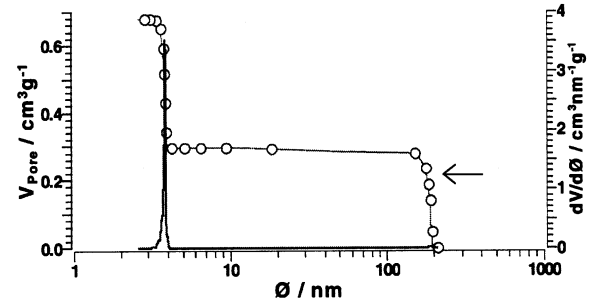

Figure 12. A plot of BJH pore distribution of silogel@5%Pt.

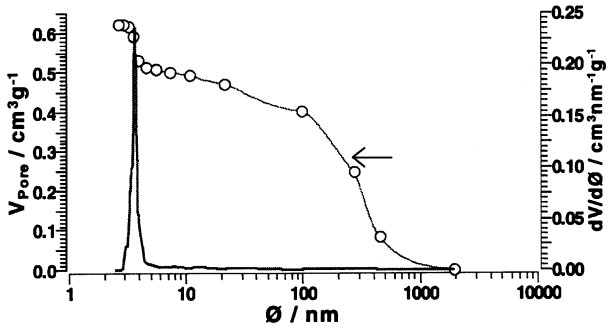

Figure 13. A plot of BJH pore distribution of silogel@5%Pt−2-alumina.

BJH Pore Distribution Analysis. As a potential supported metal catalyst synthesis technique, it is vitally important to evaluate pore structures of the unsupported and supported nanocomposites produced from this method. Figures 12−14 show typical cumulative pore volume and pore size distribution

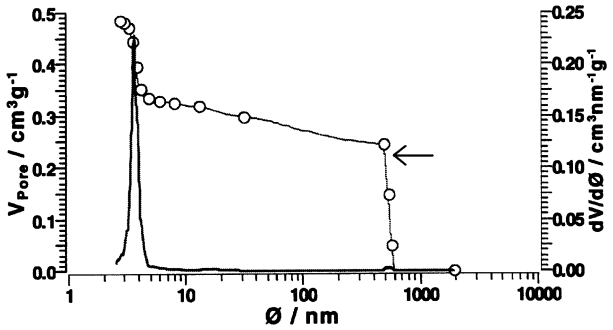

Figure 14. A plot of BJH pore-size measurement for alumina support.

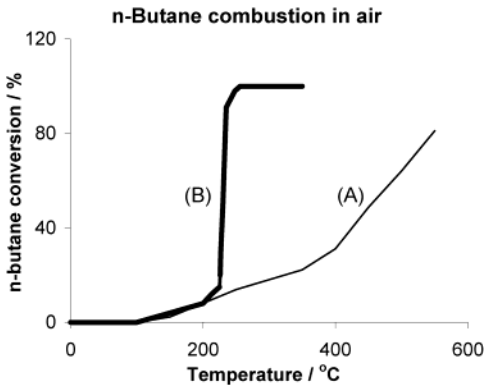

Figure 15. A plot showing the increase in butane conversion at increasing temperature over the (A) silogel@5%Pt material and (B) silogel@5%Pt−2-alumina.

curves; their calculations were based on the N_2 desorption data of p/p^0 from 1 to 0.3 with standard isotherm according to the literature.[26]

The sharp pore size distribution from Figure 12 of the sample silogel@5%Pt is denoted indicative of the very uniform pore diameter in the sol−gel coating of around 3.79 nm (more than 53.8% of the total pore volume of ~0.65 cm^3g^{-1} is contributed from these uniform pores). The pore diameter at ~110 nm is attributed to the void created between the discrete composites stacked together. Figure 14 shows the control experiment using conventional alumina support material. It is noted that this support material shows a much gentler distribution in pore size. Only 20% of the total volume of ~0.5 cm^3/g is contributed from pore diameters between 3 and 5 nm range with a much broader distribution. Pore sizes ranging from 3 to 100 nm are evident (a gentle curve) within the microparticle and ≥600 nm voids exist between the alumina particles. Deposition of the silogel@5%Pt nanocomposites onto alumina (Figure 13) shows clearly the intrinsic sharp pore at 3.79 nm associated with the porous sol−gel coating. Modification of the porosity of the alumina support (micropores within and between microparticles) by the immobilized nanocomposites is clearly evident from the gradual changes in the pore size ranging from 3 to 1000 nm.

Catalytic *n*-Butane Combustion in Air. Evaluation of the materials for catalytic *n*-butane combustion has been conducted. Typically, as shown in Figure 15, butane concentration (3500 ppm) remained unchanged until the temperature reached the light-off temperature at which the butane was rapidly converted to CO_2. It was found that the silogel@metal samples with and without support were active for catalytic combustion of *n*-butane in air. As shown in Figure 15, the general light-off temperature range for most silogel@5%metal catalysts was at about 200−250 °C, which is among the most active metal catalysts tested under similar testing conditions.[27] Figure 15A shows the reaction curve displayed by the unsupported nanocomposites, silogel@5%Pt as the catalyst. The apparent activation energy was calculated to be 25 kJ/mol. This low value strongly indicates that the reaction was in the diffusion-controlled regime. On the other hand, Figure 15B shows the reaction curve displayed by the same nanocomposites but dispersed on alumina support (silogel@5%Pt−2-alumina). Despite the dilution, the supported catalyst apparently gave higher activity at elevated temperatures. The activation energy of this catalyst was calculated to be 380 kJ/mol. This clearly indicates that the silogel@5%Pt on its own suffered a slow mass transfer of because of the clustering of the nanocomposites as aggregates rather than any accessibility problems (porosity) of the individual composites. Hence, when these composite particles are properly dispersed, the reaction could return back to the chemical-controlled regime. Although at this stage, the presented reactivity data over this type of encapsulated noble metal composites on butane oxidation are rather preliminary and far from complete where more detailed characterization (stability, structural, and morphological changes, if any, after the test) and comparison with conventional metal catalysts should be conducted, the oxidation reaction dependence on a chemical-controlled regime over these supported composites can be demonstrated. Detailed comparison of butane combustion activity of catalysts prepared by different methods at different metal loadings with and without supports will be published elsewhere.

Discussion

Three main challenges that are important in the area of supported metal catalyst synthesis are (i) the development of methods for controlling metal nanoparticle size, size distribution, composition, and perhaps even particle shape, (ii) stabilizing the metal nanoparticle on support surface by eliminating aggregation without blocking most of the active sites on the nanoparticle surfaces, and (iii) allowing independent optimization of metal−support interaction away from the choice of support (powder, pellet, monolith) used for practical considerations (mechanical, thermal, solvent stability).

Our idea was to develop generic metal nanoparticle (controlled size, composition) precursors in solutions that can be used for deposition on a wide range of support materials of different properties (wash-coat technique). Therefore, they should (a) contain no organic stabilizers, (b) be colloidally metastable in solution by the assistance of the external nanoparticle coating, (c) be easy to anchor to conventional supports, and (d) introduce no diffusion problems. We used a microemulsion technique for the initial preparation of defined metal particles using organic surfactant followed by chemical reduction. We obtained 3−5 nm monodispersed monometallic or bimetallic nanoparticles of defined size and composition (Pd, Pt, Pt−Ag) using $W = 30$. Despite a small degree of variation in their size characterized by independent techniques (XRD, CO chemisorption, TEM techniques with different capabilities & limitations), noble metal and bimetallic particles can be made in a nanometric regime with a sharp size distribution (refer to Figure 8E) using the microemulsion technique. Furthermore, control in metal particle sizing can be fine-tuned using different *W* and types of surfactants as presently demonstrated and as indicated from the literature.[4]

The key importance of this research was to determine whether the organic surfactant molecules stabilizing these nanoparticles can be replaced with an ultrathin metal sol−gel oxide coating without leading to precipitation. Thus, an extremely thin aerogel coating was applied to these colloids based on hydrolysis/

condensation of the sol−gel precursors at the micelle interface prior the removal of the surfactant. The purposes of the thin coating are to stabilize the metal clusters against agglomerization upon subsequent surfactant removal and to give surface functionality for subsequent anchoring to support materials. The coating must be thin and porous enough allowing efficient mass transfers of molecules. We show from the TEM, EDX, porosity measurement, CO chemisorption, and catalysis study that the aerogel coating on ∼5 nm metal particles exists (from directing TEM imaging and from the EDX analysis of individual colloid particles) and it is also extremely thin (thickness of ∼2.5 nm as observed directly from TEM) and porous (average pore diameter of 3.79 nm) thus posing no major problem for the inner metal site accessibility.

It is also interesting to point out that the small quantity of water and sol−gel precursor and the procedures that we developed in our case do not destabilize the inverse micelle structure as reported by Matino et al.[3] as they observed a much larger particle size formation in sol−gel embedded gold particles using a large concentration of sol−gel precursors. In addition, our ultrathin-aerogel-coated metal nanoparticles remained colloidally stable and accessible rather than those particles prepared by extensive sol−gel processing with themselves buried deep inside the sol−gel matrix.[28] It is believed that the reverse micelle aggregates present in the solution are not affected by the addition of small TEOS molecules or by subsequent reactions. The TEOS alkoxide molecules may have interacted rapidly with the small amounts of water molecules inside the reversed micelles, forming partially hydrolyzed species. These hydrolyzed species remain bound to the micelles because of their enhanced amphiphilic character brought about by the formation of silanol groups. All further reactions are therefore restricted to the micelle region. As in typical sol−gel chemistry, the size and the porosity of the coating may be further controlled by the relative amount/rates of hydrolysis and condensation of sol−gel precursors. It is noted that the key important findings from the present work are the clear demonstrations of the total extraction of organic surfactant molecules from the composites without disturbing their colloidal stability. It is thought that after gelation the surfactant molecules must be somehow trapped inside the thin aerogel coating. The pore size of this coating found is shown to resemble the pore structures in the sol−gel process using similar water/TEOS ratios.[15] Thus, these pores allow surfactant molecules to be extracted readily using hot ethanol solution, similar to the extraction of the same surfactant molecules from sol−gel,[4] MCM-41, and related structures.[29] We therefore show that the coated metal nanoparticles are stable as colloids in ethanol solution indicating the surface aerogel −OH groups and their solvent interactions can still allow their dispersion in solution because of the dominant surface polarity.

Regarding the accessibility of the aerogel coating, the TEM result indicates an ultrathin coating, which may not impose a thick diffusion pathway. The pore size measurement reflects that our samples are porous in nature. Although CO chemisorption indicates the problem of losing metal sites upon the nanocomposites immobilized onto alumina, we believe that this could be due to the artifacts introduced because of the improper prereduction (existence of a thin oxide layers on the surface of the metal particle) or simply because the supported composites may have been exposed to a high temperature hence sintering occurs (at the interface between the composites and the support, which reduces the accessibility of the metal cores). Nevertheless, CO chemisorption clearly shows that a high metal surface area (69.6 m^2 g^{-1}) can be obtained over the typical unsupported silogel@5%Pd sample. The calculated 3.59 nm particle is in excellent agreement with the result obtained from XRD (3.9 nm), clearly suggesting that the supported aerogel-coated composites are fully accessible by small molecules such as H_2 and CO. The aerogel-coated nanometal composites can then be deposited onto conventional support materials of superior support properties through surface condensation reactions.

Thus, as chemical precursor entities, we show that the soluble precursors with defined coated nanometal particles are small enough to diffuse into and anchor onto the internal and external porous structures of the support materials (from the TEM and pore analyses). There are many envisaged advantages in developing these chemical precursors. These include the rich chemical diversity and versatility of the method in controlling metal particle size, composition, coating thickness, porosity, etc. Other components (such as cerium) can also be added together with the metal precursor(s) inside the reversed micelles or as a sol−gel precursor (the use of cerium alkoxide) to develop an optimum local metal−support interaction and to relax the demands of support for other practicality reasons. We believe that this new nanotechnology in catalyst preparation and the new concepts may find useful applications.

Conclusion

To summarize, our results agree with the recent literature that the microemulsion method using reversed micelles is able to tailor metal particles (Pt, Pd) to nanometric size with a sharp particle distribution approaching monodispersity. In this work, we show that the technique can be widened to synthesis defined nanosized metal alloys (Pt−Ag) that display a truly alloy composition with no observed phase segregation of individual metal components. An extremely thin but porous layer of sol−gel coating on the metal nanocrystallites facilitating the inner metal sites accessibility without significant diffusion problems is now demonstrated. Total extraction of organic surfactant molecules can also be achieved. The inorganic metallic composites can also be maintained as a metastable colloidal state (in solution). It is therefore demonstrated that the sol−gel-coated (silogel/ceria gel) metallic nanoparticles covered with external surface −OH groups can be regarded as discrete chemical entities for attachment to solid support surfaces hence delivering new practical metal-supported catalysts without much metal aggregation/transfer problems. Thus, optimizations of metal-coating interactions and support properties could be pursued separately.

Acknowledgment. We are grateful to Johnson Matthey, plc, for the financial support and a studentship to K.M.K.Y.

References and Notes

(1) Claus, P.; Brückner, A.; Mohr, C.; Hofmeister, H. *J. Am. Chem. Soc.* **2000**, *122*, 11430.
(2) Kozlov, A.-I.; Kozlova, A.-P.; Asakura, K.; Matsui, Y.; Kogure, T.; Shido, T.; Iwasawa Y. *J. Catal.* **2000**, *196*, 56.
(3) Martino, A.; Yamanaka, S. A.; Kawola, J. S.; Loy, D. A. *Chem. Mater.* **1997**, *9*, 423.
(4) Li, T.; Moon, J.; Morrone, A. A.; Mecholsky, J. J.; Talham, D. R.; Adair, J.-H. *Langmuir* **1999**, *15*, 4328.
(5) Paulus, U.-A.; Endruschat, U.; Feldmeyer, G.-J.; Schmidt, T.-J.; Bonnemann, H.; Behm, R.-J. *J. Catal.* **2000**, *195*, 383.
(6) Okitsu, K.; Nagaoka, S.; Tanabe, S.; Matsumoto, H.; Mizukoshi, Y.; Nagata, Y. *Chem. Lett.* **1999**, *3*, 271.
(7) Papp, S.; Dekány, I. *Colloid Polym. Sci.* **2001**, *279*, 449.
(8) Hwang, C.-B.; Fu, Y.-S.; Lu, Y.-L.; Jang, S.-W.; Chou, P.-T.; Wang, C.-R.-C.; Yu, S.-J. *J. Catal.* **2000**, *195*, 336.
(9) Wu, K.-T.; Yao, Y.-D.; Wang, C.-R.-C.; Chen, P.-F.; Yeh, E.-T. *J. Appl. Phys.* **1999**, *85*, 5959.

(10) Andres, R.-P.; Bielefeld, J.-D.; Henderson, J.-I.; Janes, D.-B.; Kolagunta, V.-R.; Kubink, C.-P.; Mahoney, W.; Osifchin, R.-G.; Reifenberger, R. *Science* **1996**, *273*, 1690.
(11) Crooks R. M.; Zhao, M.; Sun, L.; Chechik, V.; Yeung, L. K. *Acc. Chem. Res.* **2001**, *34*, 181.
(12) Moser, W. R., Ed.; *Advanced Catalysts and Nanostructured Materials: Modern Synthetic Methods*; Academic Press: San Diego, CA, 1996.
(13) Maye, M. M.; Lou, Y.; Zhong, C.-J. *Langmuir* **2000**, *16*, 7520.
(14) Ikeda, M.; Tago, T.; Kishida, M.; Wakabayashi, K. *Chem. Commun.* **2001**, *23*, 2512.
(15) Zou, W.-Q.; Gonzalez, R.-D. *J. Catal.* **1995**, *152*, 291.
(16) Hanaoka, T.; Hayashi, H.; Tago, T.; Kishida, M.; Wakabayashi, K. *J. Colloid Interface Sci.* **2001**, *235*, 235.
(17) Brinker, C. J.; Scherer, G. W. *Sol−Gel Science*; Academic Press: London, 1990.
(18) Torigoe, K.; Nakajima, Y.; Esumi, K. *J. Phys. Chem.* **1993**, *97*, 8304.
(19) Dresco, P. A.; Zaitsev, V. S.; Gambino, R. J.; Chu, B. *Langmuir* **1999**, *15*, 1945.
(20) Liu, H.-F.; Mao, G.-P.; Meng, S. *J. Mol. Catal.* **1992**, *74*, 275.
(21) Durussel, P.; Feschotte, P. *J. Alloys Compd.* **1996**, *239*, 226.
(22) Wyckoff, R. W. G. *Crystal Structures*, 2nd ed.; Interscience: New York, 1963.
(23) Legrand, A. P., Ed. *The Surface Properties of Silicas*; John Wiley & Sons: Chichester, England, 1998.
(24) Beck, A.; Horváth, A.; Szücs, A.; Schay, Z.; Horváth, Z.-E.; Zsoldos, Z.; Dékány, I.; Guczi, L. *Catal. Lett.* **2000**, *65*, 33.
(25) Hernandez, C.; Pierre, A.-C. *J. Sol-Gel Sci. Technol.* **2001**, *20*, 227.
(26) Barrett, E. P.; Joyner, L. G.; Halenda, P. P. *J. Am. Chem. Soc.* **1951**, *73*, 373.
(27) Bulpitt, C.; Tsang, S.-C. *Sens. Actuators, B* **2000**, *69*, 100.
(28) Selvan, S.-T.; Nogami, M.; Nakamura, A.; Hamanaka, Y. *J. Non-Cryst. Solids* **1999**, *255*, 254.
(29) Kresge, C.-T.; Leonowicz, M.-E.; Roth, W.-J.; Vartuli, J.-C.; Beck, J.-S. *Nature* **1992**, *359*, 710.